Virtual photon theory in electrofission

F. Zamani-Noor
Villanova University, Villanova, Pennsylvania 19085

D. S. Onley
Ohio University, Athens, Ohio 45701

(Received 2 December 1985)

The process of nuclear fission induced by electrons or other charged leptons is analyzed using distorted electron wave functions and interpreted in terms of virtual photon exchange, thus relating electrofission to photofission. Comparison of cross sections and fission fragment angular distributions for photofission, electrofission, and positrofission is shown to lead to reasonable conclusions in terms of the contributions of different multipoles and intermediate states. The effects of electron distortion are found to be considerable. As a method of analysis of fission, especially near threshold, inclusive and exclusive electrofission experiments and also the ratio of electron to positron cross sections promise good results.

I. INTRODUCTION

Photons were used to induce fission in uranium and thorium as early as 1941 (Refs. 1 and 2) and yet, despite many experiments since that time, there still remain discrepancies in the photofission cross sections; compare for example results from Refs. 3 and 4 summarized in Fig. 1. Recently there have been a number of experiments using electron and positron scattering as the excitation mechanism,[5–8] and by interpreting the leptons as a source of virtual photons, we can add these to the available photofission data in the hope of clarifying the situation. Unfortunately these data are not without discrepancies also (see Fig. 2). In addition to cross section and fission-fragment angular distribution results, we have the added possibility, in the case of electrons, of analyzing correlations involving the scattered electron and a fission fragment in coincidence.[9,10] We may also anticipate the use of muons to induce fission in a similar fashion.

In view of the above considerations there seems to be a need for a reliable and flexible program of analysis for a charged lepton interacting with a fissionable target nucleus; one which will enable us to compare existing results for photofission with electrofission and to compare electrofission with positrofission and moreover to make some preliminary examination of the value of coincidence measurements. On the face of it this is a straightforward undertaking since the interaction is electromagnetic in every case and the nuclear matrix elements involved must surely be related. The process does pose some special problems because the energies of interest reach down to threshold

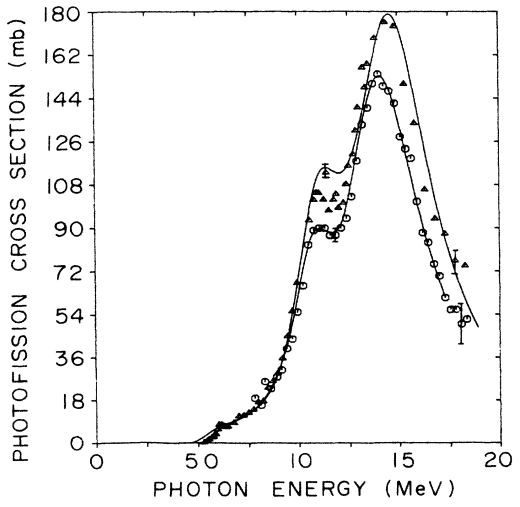

FIG. 1. Photofission cross sections for ^{238}U. The triangles and upper curve are from Ref. 3 and the circles and lower curve are from Ref. 4. Representative error bars only are shown.

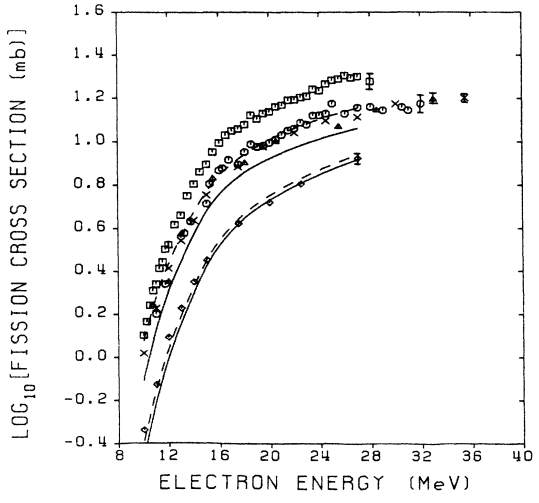

FIG. 2. Electrofission of ^{238}U from Ref. 5 (squares), Ref. 6 (triangles), Ref. 7 (circles), and Ref. 8 (diamonds). Representative error bars only are shown. Solid curves show fits using $E1$ only and dashed curves include $E2$.

(typically about 5 MeV) while the nuclei of interest are almost exclusively heavy, a combination which leads to large distortion of the electron wave function thus rendering plane-wave Born approximation inadequate. We may also have particular concern for distortion effects in the case of differential cross sections which represent only a very small slice of the total and consequently are vulnerable to small changes in the wave functions. This would be the case for example with a triple differential cross section in scattering angle, fragment emission angle, and energy.

In Sec. II of the present work we present expressions for the cross sections for different classes of experiment, namely exclusive experiments (where both electron and fission fragment are detected), inclusive experiments (fission fragments only detected), and finally the electron cross section alone with the direction of the fission fragment integrated over. We will find that it is one thing to write an expression and quite another to render the results in numerical form while preserving a respectable level of precision. At the very least we strive to avoid introducing approximations in the treatment of the electrodynamics of the problem.

The techniques for evaluating the needed cross sections are discussed in Sec. III, although to avoid exhausting the patience of the reader much of the detail is deferred to an Appendix. We compare our results with some existing experimental data in Sec. IV. We also make a few remarks on what one may expect in the analysis of different types of experiments focusing largely on the effects of the electron distorted-wave treatment as opposed to the plane-wave treatment.

II. FORMALISM FOR ELECTROFISSION

Consider the following reaction:

$$e+N\rightarrow e'+N^*\rightarrow e'+f_1+f_2\ , \tag{1}$$

where an electron e interacts with the nucleus N through the agency of virtual photon(s) and is scattered while exciting the nucleus to state N^*. The excited nucleus then decays by fission into fragments f_1 and f_2. In Fig. 3 we show the vector diagram of the process, where $\mathbf{k}_1$ is the momentum of the incoming electron, with energy E_1; it also defines the z axis. The vector $\mathbf{k}_2$ is the momentum of the outgoing electron (energy E_2), which makes an angle θ_e with the z axis; $\mathbf{k}_1,\mathbf{k}_2$ define the x-z plane. The vector $\mathbf{q}=\mathbf{k}_1-\mathbf{k}_2$ is the momentum transferred to the nucleus making an angle θ_q with the z axis. Vector $\mathbf{f}$ is the direction of one of the fission fragments, and this makes an angle θ_f with the z axis and has an azimuthal angle ϕ_f. The other fragment will be emitted in the opposite direction if we can ignore nuclear center of mass motion. Other parameters used are $\omega=E_1-E_2$, the energy transfer, and L,M the quantum numbers of the angular momentum transferred.

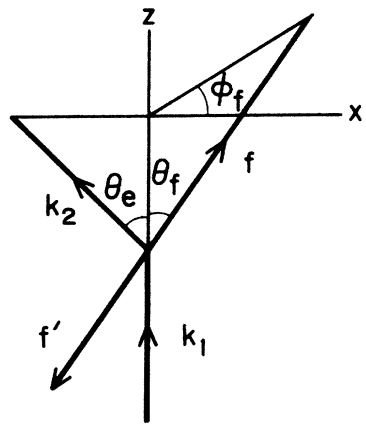

FIG. 3. Vector diagram showing the angles used in text: k_1,k_2 are the incoming and outgoing electron momenta and lie in the x-z plane. Vectors f,f' are the fission fragment directions with polar angles θ_f,ϕ_f with respect to the z-x axes.

Fission will be regarded as a two-step process. The first is the excitation of the nucleus from the ground state (treated as 0^+ throughout this paper) to a resonant state with spin (parity) L (π), while the electron is scattered in some specific direction. Next the nucleus deforms in an axially symmetric fashion, elongating along the symmetry axis and ultimately dividing into two. In the immediate prescission stage the nucleus has the structure resembling that of a symmetric top and under suitable circumstances may be accorded the set of quantum numbers L, M, and K associated with a rigid rotor.

Since we are using distorted-wave methods to treat the scattering electron, the first part of the process must be broken down into partial-wave amplitudes, $R^{\lambda L}(\kappa_1,\kappa_2)$ (see Ref. 11), which are defined to be the probability amplitudes for the electron to change from angular momentum state κ_1 (where κ is the Dirac angular momentum quantum number) to state κ_2 while emitting a photon in the multipole state $\lambda L,M$. Here λ is a label distinguishing electric multipole (E) and magnetic multipoles (M). Define $\mathscr{A}^{\lambda L}_{Mm_1m_2}$ to be the probability amplitude for the excitation of the nucleus while the electron scatters through angle θ_e; the initial and final electron spin projections are m_1,m_2. We can relate the two amplitudes by

$$\mathscr{A}^{\lambda L}_{Mm_1m_2}(\theta_e)=4\pi\omega\left[\alpha(E_1+m)(E_2+m)\frac{k_2}{E_1V}\right]^{1/2}\mathcal{N}_{\lambda L}(\omega)\frac{1}{2L+1}\sum_{\kappa_1}\sum_{\kappa_2}g^{\kappa_1\kappa_2}_{Mm_1m_2}Y^{m_1+M-m_f}_{l_2}(\theta_e,0)R^{\lambda L}(\kappa_1,\kappa_2)\ , \tag{2}$$

where

$$g^{\kappa_1\kappa_2}_{Mm_1m_2}=e^{i(\delta_{\kappa_1}+\delta_{\kappa_2})}i^{l_1-l_2}(-1)^{j_1+(1/2)}[(2l_1+1)(2j_1+1)]^{1/2}$$

$$\times C(l_1,\tfrac{1}{2}j_1;0,m_1)C(l_2,\tfrac{1}{2},j_2;m_1+M-m_2,m_2)C(j_1,j_2,L;-\tfrac{1}{2},\tfrac{1}{2})C(j_1,L,j_2;m_1,M)\ . \tag{3}$$

The quantity $\mathcal{N}_{\lambda L}$ is the reduced nuclear matrix element for the transition, and $C(\cdots)$ is the Clebsch-Gordan coefficient. Other electron angular momentum quantum numbers l_i, j_i are dependent on κ_i; the relation is given in the Appendix, Eq. (A3), where our notation for Dirac Coulomb wave functions is specified. The quantity V is the normalization volume.

In the second step, the division of the nucleus, the state of the nucleus requires the specification of the direction of the nuclear principal axes with respect to the space-fixed set of axes of Fig. 3. The Euler angles between these sets of axes, ϕ_f, θ_f, and ψ_f, are the dynamic coordinates of the top which then is described by the wave function

$$\Psi^L_{MK}(\phi_f,\theta_f,\psi_f)=\left[\frac{2L+1}{8\pi^2}\right]^{1/2} D^L_{MK}(\phi_f,\theta_f,\psi_f)\ , \quad (4)$$

where D^L_{MK} is the rotation operator

$$D^L_{MK}(\phi,\theta,\psi)=e^{iM\phi}d^L_{MK}(\theta)e^{iK\psi} \quad (5)$$

and

$$d^L_{MK}(\theta)=[(L+M)!(L-M)!(L+K)!(L-K)!]^{1/2}\sum_n \frac{(-1)^M[\sin(\theta/2)]^{K-M+2n}[\cos(\theta/2)]^{2L-K+M-2n}}{(L-K-n)!(L+M-n)!(n+K-M)!n!}\ . \quad (6)$$

Taking the symmetry axis of the top to coincide with the ultimate direction of emission of the fission fragments, we can see the probability of emission of the fragments within a solid angle $d\Omega_f$ around the direction θ_f,ϕ_f while the electron is scattered within solid angle $d\Omega_e$ around polar angle θ_e is

$$\frac{d^3P}{d\Omega_e d\Omega_f d\psi_f}=\frac{2L+1}{8\pi^2}\times\left|\sum_M \mathcal{A}^{\lambda L}_{Mm_1m_2}(\theta_e)D^L_{MK}(\phi_f,\theta_f,\psi_f)\right|^2 . \quad (7)$$

In the foregoing equations the angle ψ_f represents the nuclear rotation about the symmetry axis, which is not observable and has to be integrated over. To get the coincident cross section we divide by the incident electron flux, k_1/E_1V, and sum over spin projections thus giving us

$$\frac{d^2\sigma}{d\Omega_e d\Omega_f}=\frac{2L+1}{8\pi}\frac{E_1V}{k_1}\times\sum_{m_1}\sum_{m_2}\left|\sum_M \mathcal{A}^{\lambda L}_{Mm_1m_2}e^{iM\phi_f}d^L_{MK}(\theta_f)\right|^2 . \quad (8)$$

Now the reduced nuclear matrix element does not depend on any of the summation indices in Eq. (8) and so can be factored out to give us an equation of the form

$$\frac{d^2\sigma}{d\Omega_e d\Omega_f}=\frac{2L+1}{8\pi}|\mathcal{N}_{\lambda L}(\omega)|^2\times\sum_{m_1}\sum_{m_2}\left|\sum_M b^{\lambda L}_{Mm_1m_2}e^{iM\phi_f}d^L_{MK}(\theta_f)\right|^2 , \quad (9)$$

where

$$b^{\lambda L}_{Mm_1m_2}=4\pi\omega[\alpha(E_1+m)(E_2+m)k_2/k_1]^{1/2}/(2L+1)\times\sum_{\kappa_1}\sum_{\kappa_2} g^{\kappa_1\kappa_2}_{Mm_1m_2}Y^{m_1+M-m_2}_{l_2}(\theta_e,0)R^{\lambda L}(\kappa_1,\kappa_2)\ . \quad (10)$$

The photoabsorption cross section for the same process depends on the same factor $|\mathcal{N}_{\lambda L}|^2$ as in Eq. (9), specifically

$$\sigma^{\lambda L}_\gamma=\frac{8\pi^3}{\omega}|\mathcal{N}_{\lambda L}(\omega)|^2\delta(\omega-\omega_\gamma) \quad (11)$$

and so if we define a reduced cross section by

$$\mathcal{W}^{\lambda L}_K(\Omega_e,\Omega_f)=\frac{(2L+1)\omega^2}{64\pi^4}\times\sum_{m_1}\sum_{m_2}\left|\sum_M b^{\lambda L}_{Mm_1m_2}(\theta_e)e^{iM\phi_f}d^L_{MK}(\theta_f)\right|^2 \quad (12)$$

we can rewrite Eq. (9) as

$$\frac{d^2\sigma}{d\Omega_e d\Omega_f}=\int \mathcal{W}^{\lambda L}_K(\omega_\gamma)\sigma^{\lambda L}_\gamma(\omega_\gamma)\frac{d\omega_\gamma}{\omega_\gamma} \quad (13)$$

which expresses the electron cross section directly in terms of the photon cross section. Whereas we have performed our analysis for a single isolated resonance of energy ω and quantum numbers λLK, we can evidently complete Eq. (13) by summing over all resonances which comprise the complete photofission cross section.

The expression of Eq. (13) may be somewhat misleading; by introducing the photonuclear cross section explicitly, we do not mean to imply that the factor $\mathcal{W}^{\lambda L}_K$ in the equation is entirely independent of the nuclear model. To calculate the radial integrals $R^{\lambda L}(\kappa_1,\kappa_2)$ we still need to specify shapes for the charge and current distributions of the nucleus.

To obtain the angular distribution of fission fragments alone we integrate over electron angles in Eq. (10) and get a result which is conveniently expressed in the form of a sum over M, the projection of the transferred angular momentum along the beam direction:

$$W^{\lambda L}_K(\Omega_f)=\sum_M N^{\lambda L}_M(E_1,\omega)V^L_{MK}(\theta_f)\ , \quad (14)$$

where

$$N_M^{\lambda L}(E_1,\omega)=\frac{\omega^4\alpha}{\pi(2L+1)}(E_1+m)(E_2+m)\frac{k_2}{k_1}\times\sum_{m_1}\sum_{m_2}\left|\sum_{\kappa_1}\sum_{\kappa_2}g_{Mm_1m_2}^{\kappa_1\kappa_2}R^{\lambda L}(\kappa_1,\kappa_2)\right|^2 \quad (15)$$

is the virtual photon spectrum carrying angular momentum L with z component M, and

$$V_{MK}^L(\theta_f)=\frac{2L+1}{2}\,|\,d_{MK}^L(\theta_f)\,|^2 \quad (16)$$

is the angular distribution of fission fragments from the nuclear state with quantum numbers L, M, and K.

In photofission the quantum number M is always ±1 corresponding to the two possible states of polarization of the photon. Each nuclear substate with a distinct L,K then has a distinctive angular distribution. For electrons the quantum number M is not restricted and the relative weighting of the different M substates is a feature of the virtual photon spectrum. The angular distribution of the fission fragments when the outgoing electron is not observed is then

$$\frac{d\sigma}{d\Omega_f}=\int\sum_M\sigma_\gamma^{\lambda L}(\omega)N_M^{\lambda L}(E_1,\omega)V_{MK}^L(\theta_f)\frac{d\omega}{\omega}\,. \quad (17)$$

Notice that the angular distribution tends to be smoothed out by two processes; the sum over M which we have already noted is not present for real photons, and the sum over different contributing resonances, λL, which means that we can only expect to see an anisotropic angular distribution where these are very restricted (as in the neighborhood of threshold) or when one resonance is dominant.

For the angular distribution of the outgoing electrons we integrate over the fission fragment angles in Eq. (12) and one then gets the electron differential cross section,

$$\frac{d\sigma^{\lambda L}}{d\Omega_e}=\frac{1}{2}\frac{k_1}{E_1V}\sum_{m_1}\sum_{m_2}\sum_M|\,\mathscr{A}_{Mm_1m_2}^{\lambda L}\,|^2\,. \quad (18)$$

To get the total electrofission cross section, we integrate over both electron and fission fragment angles with the result

$$\sigma^{\lambda L}(E_1)=\tfrac{1}{2}(4\pi\omega)^2\alpha^2(E_1+m)(E_2+m)\frac{k_2}{k_1}\,|\,\mathscr{N}_{\lambda L}\,|^2(2L+1)^{-1}\sum_{m_1}\sum_{m_2}\sum_M\left|\sum_{\kappa_1}\sum_{\kappa_2}g_{Mm_1m_2}^{\kappa_1\kappa_2}R^{\lambda L}(\kappa_1,\kappa_2)\right|^2\,. \quad (19)$$

Relating this to the corresponding photon cross section, given in Eq. (9), we get the result

$$\sigma^{\lambda L}(E_1)=\int\sigma_\gamma^{\lambda L}(\omega)N^{\lambda L}(E_1\omega)\frac{d\omega}{\omega}\,, \quad (20)$$

which is very similar to what one would get for any photoprocess for which the cross section is $\sigma_\gamma^{\lambda L}$ and where the incident radiation has the spectrum $N^{\lambda L}$. In this case, of course, $N^{\lambda L}$ is the virtual photon spectrum:

$$N^{\lambda L}=\sum_M N_M^{\lambda L}$$

which reduces to

$$N^{\lambda L}(E_1\omega)=\frac{\alpha}{\pi}\frac{k_2}{k_1}\frac{(E_1+m)(E_2+m)\omega^4}{2L+1}\times\sum_{\kappa_1\kappa_2}(2j_1+1)(2j_2+1)\times|\,C(j_1j_2L;-\tfrac{1}{2},\tfrac{1}{2})R^{\lambda L}(\kappa_1,\kappa_2)\,|^2\,. \quad (21)$$

III. CALCULATION OF CROSS SECTION

The interaction between the appropriate components of the electron current and charge densities J^{EL},ρ^{EL} and those of the nuclear vector and scalar potentials A^{EL},ϕ^{EL} is written:

$$R_I^{\lambda L}(\kappa_1,\kappa_2)=\int_0^\infty(A^{\lambda L}J^{\lambda L}-\phi^{\lambda L}\rho^{\lambda L})r^2dr\,, \quad (22)$$

where the quantity $R_I^{\lambda L}$ is, aside from normalization [see Eq. (28)], the same as the radial integral $R^{\lambda L}$ introduced in Sec. II. The charge and current transition charge densities are written in terms of f_κ,g_κ, the two radial components of the Dirac wave function for the electron moving in the Coulomb field of the nucleus:

$$J^{EL}=i[L(L+1)]^{-1/2}[L(f_{\kappa_1}g_{\kappa_2}-g_{\kappa_1}f_{\kappa_2})+(\kappa_1-\kappa_2)(f_{\kappa_1}g_{\kappa_2}+g_{\kappa_1}f_{\kappa_2})]\,, \quad (23a)$$

$$J^{ML}=-i[L(L+1)]^{-1/2}(\kappa_1+\kappa_2)(f_{\kappa_1}g_{\kappa_2}+g_{\kappa_1}f_{\kappa_2})\,, \quad (23b)$$

$$\rho^{EL}=f_{\kappa_1}f_{\kappa_2}+g_{\kappa_1}g_{\kappa_2}\,. \quad (23c)$$

The nuclear current density is also broken down into multipoles,

$$\mathbf{J}_{\rm nuc}(\mathbf{r})=\sum_{M,L,L'}J_{L'}(r)\mathbf{Y}_{LL'}^M(\hat{\mathbf{r}}) \quad (24)$$

and the corresponding potentials [in the least singular gauge (Ref. 11)] are then

$$\begin{aligned}A^{EL}(r)=&h_{L-1}(\omega r)\int_0^r\{-j_{L+1}(\omega r')[L/(L+1)]^{1/2}J_{L+1}(r')+j_{L-1}(\omega r')J_{L-1}(r')\}r'^2dr'\\&+j_{L-1}(\omega r)\int_r^\infty\{-h_{L+1}(\omega r')[L/(L+1)]^{1/2}J_{L+1}(r')+h_{L-1}(\omega r')J_{L-1}(r')\}r'^2dr'\\&-[L/(L+1)]^{1/2}(2L+1)\omega^{-3}r^{L-1}\int_r^\infty J_{L+1}(r')r'^{-L}dr'\,,\end{aligned} \quad (25a)$$

$$A^{ML}(r)=h_L(\omega r)\int_0^r j_L(\omega r')J_L(r')r'^2dr'+j_L(\omega r)\int_r^\infty h_L(\omega r')J_L(r')r'^2dr' , \tag{25b}$$

$$\phi^{EL}(r)=[L/(L+1)]^{1/2}\Big[h_L(\omega r)\int_0^r\{-j_{L+1}(\omega r')[L/(L+1)]^{1/2}J_{L+1}(r')+j_{L-1}(\omega r')J_{L-1}(r')\}r'^2dr'$$
$$+j_L(\omega r)\int_r^\infty\{-h_{L+1}(\omega r')[L/(L+1)]^{1/2}J_{L+1}(r')+h_{L-1}(\omega r')J_{L-1}(\omega r')\}r'^2dr'\Big]$$
$$-[(L+1)/(2L+1)]^{1/2}r^2/\omega^2\int_r^\infty J_{L+1}(r')r'^2dr' . \tag{25c}$$

Notice that in Eqs. (25) the nuclear transition charge distribution does not appear explicitly since it can be related to the current distribution through the continuity equation. The radial functions J_{L-1} and J_{L+1} for an electric multipole transition, or J_L for a magnetic multipole transition, are thus the needed independent functions describing the nuclear participation in this stage of the interaction. The complicated forms given in Eqs. (25) arise only because the range of integration extends throughout the nucleus; once outside the nucleus (i.e., for $r>R_{\rm nuc}$ where all $J_{L'}=0$) they take on the simple forms:

$$A^{EL}=h_{L-1}(\omega r)R_N^{EL} , \tag{26a}$$

$$A^{ML}=h_L(\omega r)R_N^{ML} , \tag{26b}$$

$$\phi^{EL}(r)=[L/(L+1)]^{1/2}h_L(\omega r)R_N^{EL} , \tag{26c}$$

where R_N^{EL},R_N^{ML} are the radial parts of the nuclear transition matrix elements:

$$R_N^{EL}=\int_0^{R_{\rm nuc}}\{-j_{L+1}(\omega r')[L/(L+1)]^{1/2}J_{L+1}(r')$$
$$+j_{L-1}(\omega r')J_{L-1}(r')\}r'^2dr' , \tag{27a}$$

$$R_N^{ML}=\int_0^{R_{\rm nuc}}j_L(\omega r')J_L(r')r'^2dr' . \tag{27b}$$

If we extract the factor $R_N^{\lambda L}$ from the transition integral $R_I^{\lambda L}$, we get the radial integral,

$$R^{\lambda L}(\kappa_1,\kappa_2)=R_I^{\lambda L}(\kappa_1,\kappa_2)/R_N^{\lambda L} , \tag{28}$$

which is now identical to that used in Eq. (2).

To calculate the radial integral in Eq. (22), we need to perform an integral over an infinite range. The integral involves nuclear density functions for values of $r<R_{\rm nuc}$. It is known[12] that the detailed shapes are not particularly vital for virtual photon calculations in this range, which depend primarily on the values of the nuclear root-mean-square radius and the appropriate transition radius. We use here expressions derived from assuming irrotational incompressible flow in the nucleus:

$$J_{L-1}(r)=r^{L-1}\rho_0(r) ,$$
$$J_L=d\rho_0/dr ,$$
$$J_{L+1}=0 ,$$

where $\rho_0(r)$ is the ground state charge distribution which is taken to be the standard Fermi shape.

However, it is impossible to evaluate an infinite-range integral with confidence unless some analytic limits can be set on the remainder. The nature of the integrand in this case renders the convergence as the upper limit tends to infinity very slow and irregular, and so it becomes particularly important to evaluate the exterior part of the integral $r>R_{\rm nuc}$ for suitably large r, which it is possible to do in the form of an asymptotic series (see Appendix A).

Apart from the infinite integrals we also have to perform infinite sums over initial and final angular momenta κ_1,κ_2 in Eqs. (2), (9), (12), and (19) in Sec. II. When one quantum number is fixed (say κ_2) the sum over the other is restricted by selection rules, so there is an unrestricted sum over one variable only. Techniques used here depend on whether the sum is coherent or incoherent. In the expressions for the virtual photon spectrum, for example, the final sum is incoherent, that is of the form

$$N^{\lambda L}=\sum_{\kappa_2=1}^{\infty}a_{\kappa_2} . \tag{29}$$

The sum has a slow rate of convergence, as has been noted elsewhere,[13] making direct summation quite unreasonable. However, it is found that for suitably large κ_2, the terms become insensitive to the nuclear charge Z and radius R_n and may be replaced by their values in the limit $Z\to0$, $R_n\to0$, denoted here by the notation $[\cdots]_0$;

$$N^{\lambda L}=\sum_{\kappa_2=1}^{\kappa_m}a_{\kappa_2}+\sum_{\kappa_2=\kappa_m+1}^{\infty}[a_{\kappa_2}]_0 . \tag{30}$$

However, the sum of *all* terms in this limit is simply equivalent to the calculation carried out in the plane-wave and long-wavelength limits, and this is well known to result in simple analytic forms.[14,15] For example, for the electric dipole

$$[N^{E1}]_0=\frac{\alpha}{\pi}\left|\frac{(E_1+E_2)^2}{k_1^2}\right.$$
$$\left.\times\ln\left[\frac{E_1E_2-k_1k_2-m^2}{m(E_1-E_2)}\right]-\frac{2k_2}{k_1}\right| . \tag{31}$$

Thus we may write Eq. (30) in the form

$$N^{\lambda L}=[N^{\lambda L}]_0+\sum_{\kappa_2=1}^{\kappa_m}(a_{\kappa_2}-[a_{\kappa_2}]_0) \tag{32}$$

replacing the sum of Eq. (29) by one that converges very rapidly. We will now need the radial integral of Eq. (22) evaluated in this limit which presents a problem because expressions developed hitherto then become indeterminate. We give an independent evaluation of $[R^{\lambda L}(\kappa_1,\kappa_2)]_0$ in Appendix A. Expressions for $[N^{\lambda L}]_0$ in this limit are, as we have remarked, well known. However, we find no record of expressions for the corresponding

breakdown into magnetic substates $[N_M^{\lambda L}]_0$; we give expressions for these also in Appendix B.

IV. INCLUSIVE EXPERIMENTS

In Sec. II, the electrofission cross section was related to the photofission cross section $\sigma_{\gamma f}$ via the virtual photon spectrum (VPS). Measurements of $\sigma_{\gamma f}$ for ^{238}U have been made by the Saclay group[4] and by the Livermore group[5] in the photon energy range 5–19 MeV. The photoabsorption cross section is dominated by the giant dipole resonance (GDR) with peaks at approximately 11 and 14 MeV, and can be reasonably represented by two Lorentzian curves (see Refs. 3 and 4). The photofission cross section is about one-tenth of the total in this range. In Fig. 1 we compare the results obtained by the two groups and show also the analytic curves we have fitted to their data.

Although related to photofission, electrofission measures something a little different because of the relatively enhanced spectra for the multipoles beyond $E1$. To translate a photofission cross section into an electrofission cross section we would need the multipole breakdown of $\sigma_{\gamma f}$. In the giant resonance region this decomposition would be confined to a few multipoles only, and prominent among them would be the giant quadrupole resonance (GQR).[16]

We have used our VPS along with the measured photofission cross sections for ^{238}U to calculate both the electrofission and positrofission cross sections. For the GQR we have used simple Gaussians at two alternative energies:

$$\sigma_{\gamma f}^{E2}(E_\gamma)=\sigma_{\gamma f}^{E2}(E_x)\exp\left[-\left[\frac{E_\gamma-E_x}{\Gamma/2}\right]^2\ln 2\right] \tag{33}$$

with

$$\sigma_{\gamma f}^{E2}(E_x)=3.5 \text{ mb}, \quad E_x=9 \text{ MeV}, \quad \Gamma=4 \text{ MeV}, \tag{34a}$$

$$\sigma_{\gamma f}^{E2}(E_x)=11.7 \text{ mb}, \quad E_x=11 \text{ MeV}, \quad \Gamma=2 \text{ MeV}; \tag{34b}$$

these expressions represent a GQR strength of 70% of the energy weighted sum rule. The balance of the cross section is then assumed to be electric dipole. Figure 2 shows the ^{238}U electrofission measurements by a number of different groups and the sole positrofission measurement.[5–8] The solid lines show the results of our calculation if we discount the GQR, and the dashed lines show the results of including the GQR. It can be seen that the quadrupole contribution to positrofission is small, whereas the contribution to fission by electrons is considerable and essential if we are to obtain agreement; it is not possible to place the energy of the resonance more accurately, however, as either of the alternates (34a) or (34b) are equally good. Note that we have used for photofission the data of Saclay;[4] if we use the somewhat larger cross section of Livermore[3] we are unable to reach agreement even with zero quadrupole contribution. The Giessen group, who have measured both the electron and positron cross sections,[8] have taken the ratio of the two thereby avoiding any question of the normalization of the photofission cross sections, and we show the result in Fig. 4 compared with our calculations. In this comparison we find a clear preference for a GQR with the parameters of (34a); parameters (34b) or zero resonance are equally (although not overwhelmingly) unacceptable.

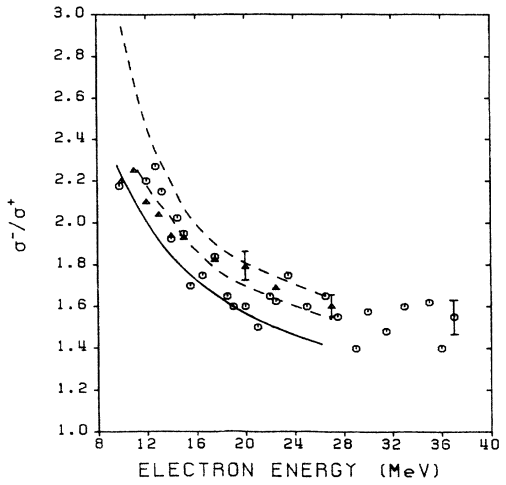

FIG. 4. The ratio of electrofission to positrofission in ^{238}U: the data are from Ref. 8. The solid curve is for $E1$ only; the lower and upper dashed curves contain $E2$ with parameters given in Eqs. (34a) and (34b), respectively.

The same experimental setup has been used to obtain angular distributions of fission fragments in a few cases and these, too, can be accounted for using our VPS calculated here. Such angular distributions, as already remarked, are only significantly anisotropic near threshold, and again the assumption has been made that there are only dipole and quadrupole components present, although unrelated to the giant dipole and quadrupole contributions discussed in the last section. For the low energy quadrupole contribution we have used an old estimate by Blatt and Weisskopf:[17]

$$\sigma_\gamma^{E2}(E)=1.2E^3\left[\frac{R}{6}\times 10^{-3}\right]^4\times 10^{-3} \text{ mb}. \tag{35}$$

The nucleus we are considering this time is ^{232}Th, and we have used photofission data from Ref. 3. In Fig. 5 we show the comparison with the measured angular distributions[18] at 9.0 MeV; we have used one variable parameter in this case; namely, the relative contributions of $K=0$ states to $K=1$ states to the fission channel.

Other angular distributions have been measured for electrofission, for example by Arruda-Neto,[19] where the distributions are fitted to the form

$$W(\theta)=a+b\sin^2\theta+c\sin^2 2\theta, \tag{36}$$

which has also been used for studying threshold photofission, and which again would result from assuming dipole and quadrupole contributions, the coefficient c coming from quadrupole alone. Reference 18 shows a plot of these coefficients as a function of electron energy for the nucleus ^{238}U, which is reproduced in Fig. 6. To interpret such curves it is necessary to assume the presence of a number of states in the transition nucleus, for example those which we show in Fig. 7. Then the result of apply-

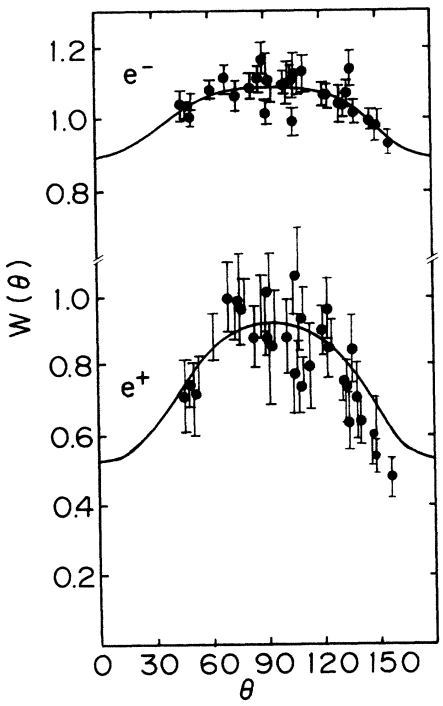

FIG. 5. Fission fragment angular distributions for ^{232}Th using electrons and positrons of energy 9.0 MeV. Data are from Ref. 18.

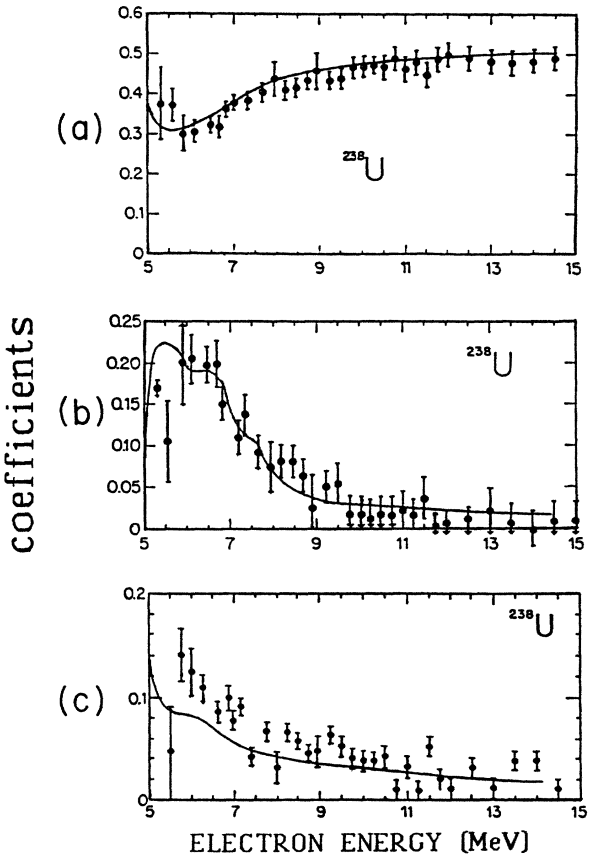

FIG. 6. Fission fragment angular distribution coefficients [see Eq. (36)] for electrofission of ^{238}U as a function of electron energy. Data are from Ref. 19. The fit assumes threshold resonances shown in Fig. 7.

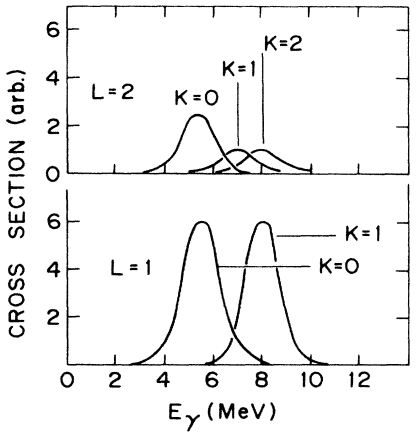

FIG. 7. Dipole and quadrupole states in the ^{238}U transition nucleus necessary to fit the angular distribution in Fig. 6.

ing the analysis of Sec. II is the fit shown as solid curves in Fig. 6; note that we have made no claim to a unique analysis of this structure; we are content to show how an interpretation can be obtained using the methods described here.

V. COINCIDENT ANGULAR DISTRIBUTIONS

Until recently it has not been possible to detect the scattered electron in coincidence with the fission fragments. Now, however, where this is possible, one could measure the angular distribution of fission fragments for a series of well defined excitation energies and momentum transfers. In the current section we will use our simple single-resonance model to examine the characteristics of the final state and interpret these in terms of the intermediate virtual photon.

In Sec. II we derived an expression giving the electron angular distribution coincidentally with the fission fragment angular distribution. In the cases considered here there is a well-defined symmetry axis to the angular distribution of fission fragments and, indeed, in simple one-photon exchange one would expect this to be coincident with the direction of the momentum transfer. It is convenient to identify the axis of symmetry which also lies in the scattering plane at angle θ_s. Fission fragment angles with respect to this axis are distinguished by a prime, θ'_f,ϕ'_f (see Fig. 8).

We show in Figs. 9(a) and (b) polar plots of the fission angular distribution expected for real photons exciting transition states with $L=1$, $K=0$ and $L=1$, $K=1$. In both cases the z axis is both the beam direction and the symmetry direction, and since the radiation is taken to be unpolarized the angular distribution is independent of the azimuthal angle. These plots are the same regardless of the photon energy.

For comparison we have calculated the fragment angular distributions for the corresponding transitions for a 20 MeV electron scattering through 40° and leaving with 15 MeV; thus this can be regarded as a 5 MeV virtual photon

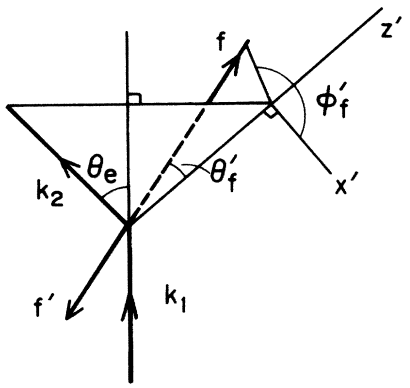

FIG. 8. Vector diagram, comparable with Fig. 3, showing fission fragment polar angles θ'_f,ϕ'_f measured from z' axis (the symmetry direction) and x' axis (perpendicular to z' axis in the scattering plane).

exchange corresponding roughly to threshold for fission of ^{238}U. In Fig. 10 we show the polar plots assuming an intermediate $M1$ state. Since an $M1$ photon is purely transverse one could expect that the results closely resemble the real photon as indeed they do. The observation that the polar plots are not in this case precisely azimuthally symmetric can be interpreted as demonstrating partial polarization of the virtual photon in the scattering plane. The comparison also yields the apparent photon direction (the appropriate symmetry axis) which is notable in that it is not the same as the momentum transfer direction (identified as q in the figures). In a single photon exchange process all of the momentum is conveyed to the nucleus by a photon which also carries the energy of excitation, thus the momentum transfer can be taken to be indicative of the direction of that photon. In the distorted-wave treatment momentum is also conveyed by the Coulomb potential between electron and nucleus in the

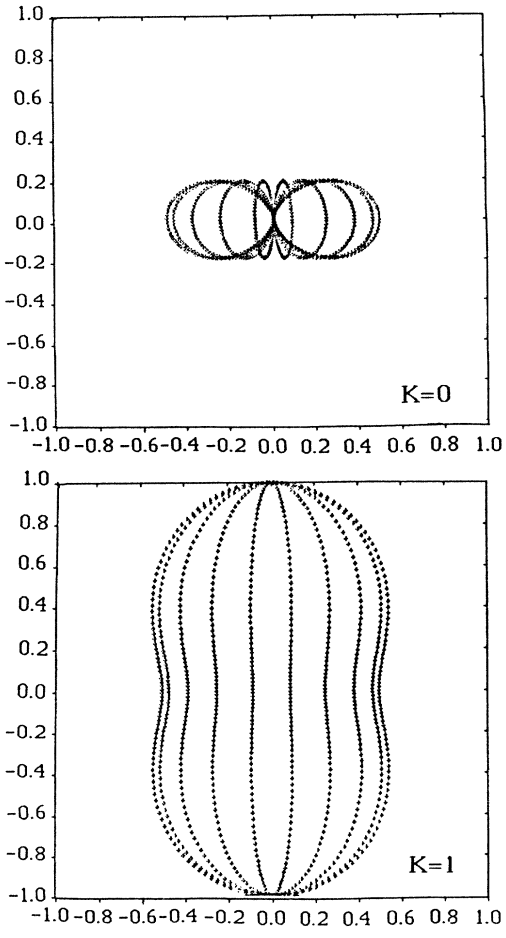

FIG. 9. Polar plots for fragment angular distributions from photofission. We assume a dipole transition state with $K=0$ (upper plot) or $K=1$ (lower plot).

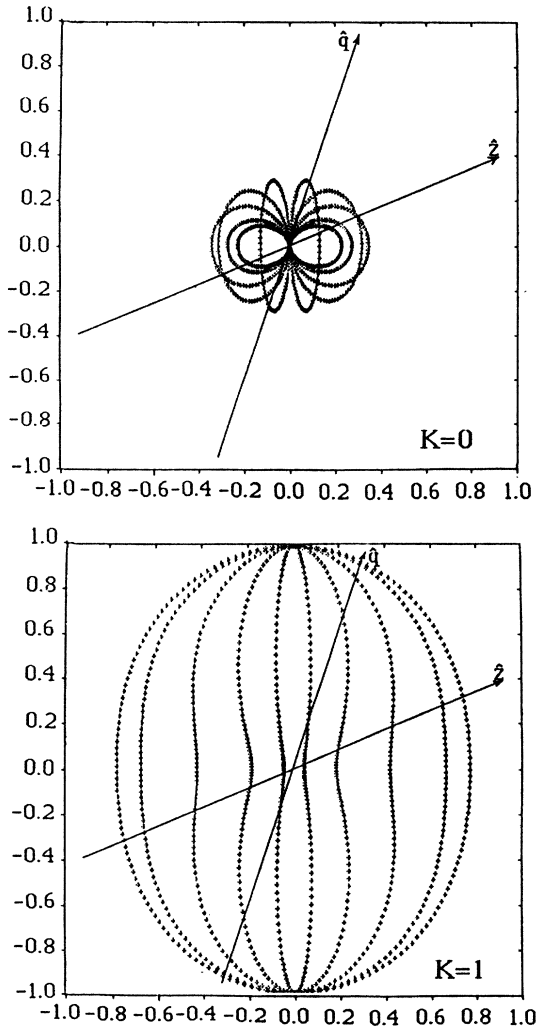

FIG. 10. Polar plots for fragment angular distributions from electrofission comparable with Fig. 9. The level assumed is $M1$ with $K=0$ or $K=1$. Electron energy is 20 MeV, the scattering angle is 40°, and excitation energy is 5 MeV.

approach and departure phases and whereas there is a single energy-bearing photon exchanged it does not carry all of the momentum.

Next we consider an intermediate $E1$ state. Compare Figs. 11 and 9, and notice that the distributions for both $K=0$ and $K=1$ are quite different: in fact they appear almost to be interchanged; this is due to the longitudinal interaction. Generally for an $E1$ transition induced by electron scattering, we find that the interaction is predominantly longitudinal except where the scattered electrons are in a narrow cone in the forward or backward directions in which case the interaction is predominantly transverse. In the $K=0$ case, for example, the fission fragments tend to be ejected in the direction of the electric vector which is perpendicular to the velocity for the real photon of Fig. 9 and along that direction for the longitudinal component of the virtual photon in Fig. 11. Notice again that the virtual photon direction is not the same as the momentum transfer direction; in this case, however,

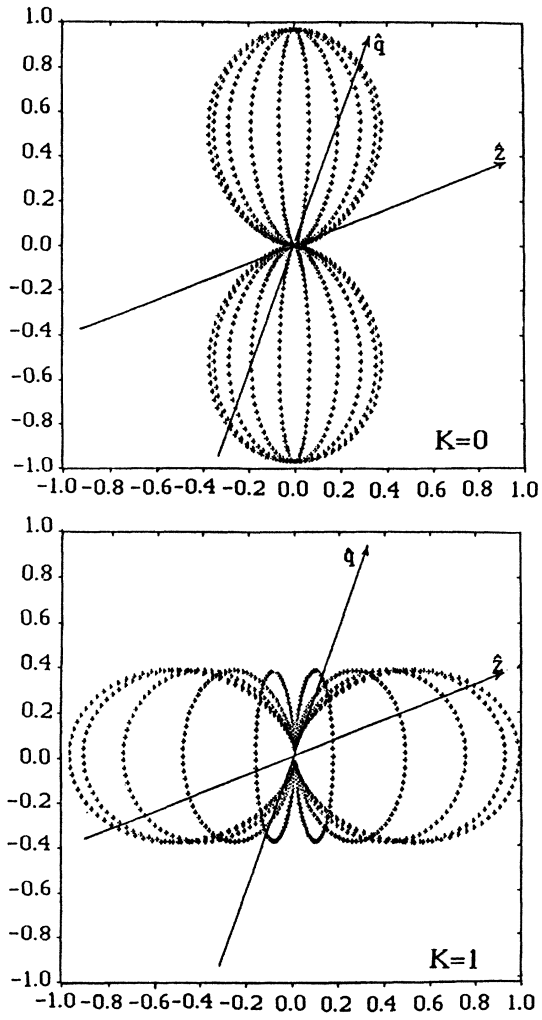

FIG. 11. Polar plots for fragment angular distribution comparable with Figs. 9 and 10. The level assumed is $E1$; all other parameters are the same as in Fig. 10.

the interaction is further complicated by the presence of both longitudinal and transverse components and it would be incorrect to assume a real-photon-like appearance to the angular distribution produced, even in the absence of distortion.

We have carried out similar calculations for the corresponding $L=2$ situation. The observations are qualitatively like those for the dipole cases, although $E2$ is slightly more complicated in having three K values and double-lobed distributions.

VI. CONCLUSION

We studied different aspects of electrofission of heavy nuclei with the object of interpreting them in terms of virtual photon transfer. Since these nuclei typically have a large radius and large charge, it is necessary to take into account both the physical extent of the nucleus and the distortion of the electron waves. We developed methods of doing the exterior radial integrals so that we were able to produce reliable electron matrix elements with precision of about 1 part in 10^7. We also are able to provide a correction procedure so that the sum over all partial waves can be taken into account. Starting with measured photofission cross sections we were able to account for exclusive electrofission and positrofission cross sections for ^{238}U with a reasonable sized $E2$ component in the photofission cross section.

We are also able to examine angular distribution of fission fragments and again for ^{238}U found that the measured distributions were compatible with a small number of transition states as seems to be the case for photofission. We found similar results for the angular distribution of fission fragments from ^{232}Th.

In the case of coincidence measurements where both the scattered electron and the fission fragments are detected we have only looked at simple single-resonance models primarily to see what characteristics of the fission fragment angular distribution we could ascribe to the spin and parity of the photon transferred. In particular we could compare these with the corresponding results for real photons and with the one-photon exchange picture with no distortion. It was clear that the presence of the longitudinal component drastically changes the distribution for electric multipole transitions and the photon direction as given by the symmetry of the angular distribution of the fission fragments is not coincident with momentum transfer direction.

ACKNOWLEDGMENTS

Calculations reported here were carried out on the CRAY XMP computer at the magnetic fusion energy computer center by arrangement with the U.S. Department of Energy. We would like to acknowledge the assistance of Ulrich Kneissl and assistants at the Institute fur Kernphysik in Giessen, for providing data and useful comments. This work was supported by the U.S. Department of Energy under Grant No. DE-AC02-79ER-10397-07.

APPENDIX A: RADIAL INTEGRALS

The time independent Dirac equation with a central potential in standard notation[20,21] is

$$[\mathbf{a}\cdot\mathbf{p}+\beta m+V(r)]\psi=E\psi\ . \tag{A1}$$

The solution when separated in polar coordinates is written as

$$\psi_\kappa^\mu=\begin{Bmatrix} g_\kappa(r) & \chi_\kappa^\mu \\ -if_\kappa(r) & \chi_{-\kappa}^\mu \end{Bmatrix}, \tag{A2}$$

where χ_κ^μ are the two-spinor angular-momentum eigenfunctions

$$\chi_\kappa^\mu=\sum_{\tau=\pm 1/2} C(l,\tfrac{1}{2},j;\mu,-\tau,\tau)Y_l^{\mu-\tau}(\theta,\phi)\chi_{1/2}^\mu\ . \tag{A3}$$

In Eq. (A3) the subsidiary angular momentum eigenvalues j and l are regarded as functions of the Dirac angular-momentum eigenvalue which specifies both

$$\begin{aligned} j&=|\kappa|-\tfrac{1}{2}\ , \\ l&=\kappa \ \text{ for } \ \kappa>0\ ; \\ l&=-\kappa-1 \ \text{ for } \ \kappa<0\ . \end{aligned} \tag{A4}$$

For the free particle $[V(r)=0]$ the radial functions with this convention reduce to

$$\begin{aligned} f_\kappa(r)&=\mathrm{sgn}(\kappa)/(E+m)j_{\bar{l}}(kr)\ , \\ g_\kappa(r)&=j_{\bar{l}}(kr)\ , \end{aligned} \tag{A5}$$

where j_l is the spherical Bessel function and $\bar{l}=l-\mathrm{sgn}(\kappa)$. For a Coulomb potential having charge Ze as its source the same functions become

$$\begin{aligned} f_\kappa&=-\frac{E-m}{k}\mathrm{Im}[V_{\pm\gamma}(kr)]\ , \\ g_\kappa&=\mathrm{Re}[V_{\pm\gamma}(kr)]\ , \end{aligned} \tag{A6}$$

where V_γ can be written as a combination of Whittaker functions of the second kind, $W_{\kappa,\mu}$, as follows:

$$V_\gamma(kr)=2(2kr)^{-3/2}\Gamma(\gamma+i\eta)(\gamma+i\eta)e^{-\pi\eta/2+i(\psi-\gamma\pi/2-\pi/4)}\left[e^{i\pi/2}\frac{W_{i\eta+(1/2),\gamma}(-2ikr)}{\Gamma(\gamma+1+i\eta)}+e^{i\pi(\gamma+1)}\frac{W_{-i\eta-(1/2),\gamma}(2ikr)}{\Gamma(\gamma-i\eta)}\right] \tag{A7}$$

with

$$\begin{aligned} \gamma&=(\kappa^2-\alpha^2Z^2)^{1/2}\ , \\ \eta&=\alpha ZE/k\ , \\ e^{2i\psi}&=e^{-i\pi}\left[\frac{\kappa-i\alpha Zm/k}{\gamma+i\eta}\right]. \end{aligned} \tag{A8}$$

The choice of sign of γ in Eq. (A7) is $(+)$ for the regular function and $(-)$ for the irregular function. Since our problem has a pure Coulomb field only outside the nucleus, the solution will be a linear combination of both regular and irregular solutions and hence combinations of $W_{\pm i\eta+(1/2),\pm\gamma}$ and their complex conjugates. Moreover, the radial integrals of Eq. (28) in the text have relatively simple forms in the same region:

$$\begin{aligned} R^{EL}=[L/(L+1)]^{1/2}\int_R^\infty &[h_L^{(1)}(\omega r)(f_{\kappa_1}g_{\kappa_2}-g_{\kappa_1}f_{\kappa_2})+(\kappa_1-\kappa_2)/Lh_{L-1}^{(1)}(\omega r)(f_{\kappa_1}g_{\kappa_2}+g_{\kappa_1}f_{\kappa_2}) \\ &-h_L^{(1)}(\omega r)(f_{\kappa_1}f_{\kappa_2}+g_{\kappa_1}g_{\kappa_2})]r^2dr \end{aligned} \tag{A9}$$

for electric transitions, and

$$R^{ML}=(\kappa_1+\kappa_2)[L(L+1)]^{-1/2}\int_R^\infty h_L^{(1)}(\omega r)(f_{\kappa_1}g_{\kappa_2}+g_{\kappa_1}f_{\kappa_2})r^2dr \tag{A10}$$

for magnetic transitions.

In order to evaluate these integrals it is evidently sufficient to have expressions for integrals of the kind

$$A=\int_R^\infty h_L(\omega r)W_{b_1d_1}(ie_1r)W_{b_2d_2}(ie_2r_2)r^{-1}dr\ . \tag{A11}$$

This is achieved in the present case by using the asymptotic expansion[22]

$$W_{b,d}(z)=e^{-(1/2)z}z^b\sum_{r=0}^{s-1}\frac{(\frac{1}{2}+b-d)_n(\frac{1}{2}-b-d)_n}{n!}(-z)^{-n}+O(z^{-s}) \tag{A12}$$

and integrating term by term. The result is a multiple sum over incomplete gamma functions

$$A=\omega^{-1}w^{-b_1-b_2+1}\sum_{m=0}\left\{(2e^{-i\pi/2})^{\beta_m}im\frac{\pi}{2}\left[\frac{w}{e_2}\right]^m(\tfrac{1}{2}+d_2-b_2)_m(\tfrac{1}{2}-d_2-b_2)_m/m!\Gamma(\beta_m,\tfrac{1}{2}iwR)\right.$$
$$\times\sum_{n_1}\left[\frac{(\frac{1}{2}+d_1-b_1)_{n_1}(\frac{1}{2}-d_1-b_1)(e_2/e_1)^{n_1}}{n_1!(\frac{1}{2}+d_2-b_2+m-n_1)_{n_1}(\frac{1}{2}-d_2-b_2+m-n_1)_{n_1}}\right.$$
$$\left.\left.\times\sum_{n=0}^{L}\frac{(1+m-n-n_1)_n(L+1)_n(-L)_n(-e_2/2\omega)^n}{n!(\frac{1}{2}+d_2-b_2+m-n_1-n)_n(\frac{1}{2}-d_2-b_2+m-n_1-n)_n}\right]\right\}, \tag{A13}$$

where

$$w=e_1+e_2-2\omega\ ,$$
$$\beta_m=b_1+b_2-1-m\ . \tag{A14}$$

We also need to evaluate the same radial integrals in the limit $Z\to 0$ and $R\to 0$. In this case the expansions (A12) terminate [in fact becoming $h_l(z)$]. The integrals (A11) diverge in the limit $R\to 0$, but the integrals we want, Eqs. (A9) and (A10), are quite regular and evidently composed of terms of the form

$$I_0=\int_0^\infty h_L^{(1)}(\omega r)j_{l_1}(k_1r)j_{l_2}(k_2r)r^2dr\ . \tag{A15}$$

Using the same techniques we get the expressions

$$I_0=\tfrac{1}{4}\sum_{n_1=0}^{l_1}\sum_{n_2=0}^{l_2}\sum_{n=0}^{l}\sum_{j=1}^{4}a_0k_1^{-n_1-1}k_2^{-n_2-1}\omega^{-n-1}c_jP_j^N\left[-\frac{\pi}{2N!}-i(-1)^{j+N}\Xi(N)+i\frac{(-1)^j}{N!}\ln P_j\right], \tag{A16}$$

where

$$a_0=2^{-N}(L+1)_n(l_1+1)_{n_1}(l_2+1)_{n_2}(-L)_n$$
$$\times(-l_1)_{n_1}(-l_2)_{n_2}/n_1!n_2!n!\ ,$$
$$N=n_1+n_2+n_3$$
$$\Xi(N)=\sum_{s=1}^{[(N+1)/2]}\left[\frac{-2N+4s-3}{(-N)_s(N-2s+2)}\right]$$
$$-\frac{1}{N!}[\tfrac{1}{2}-\gamma-(-1)^N\tfrac{1}{2}]\ ,$$
$$P_1=k_1+k_2+\omega,\quad c_1=(-i)^{l_1+l_2+L}\ ,$$
$$P_2=k_1-k_2-\omega,\quad c_2=(-i)^{-l_1+l_2+L}(-1)^{n_2+n}\ , \tag{A17}$$
$$P_3=k_1-k_2+\omega,\quad c_3=(-i)^{l_1-l_2+L}(-1)^{n_2+1}\ ,$$
$$P_4=k_1+k_2-\omega,\quad c_4=(-i)^{L-l_1-l_2}(-1)^{n_1+1}\ .$$

In Eq. (17) $[x]$ means the integral part of x.

The expression (A16) is unsuitable for numerical evaluation in many cases due to large degree of cancellation among the terms. In such cases we have been able to overcome the difficulty by reexpanding terms of the form

$$\mathscr{I}=\tfrac{1}{4}\sum_{n_1=0}^{l_1}\sum_{n_2=0}^{l_2}\sum_{n=0}^{L}a_0k_1^{-n_1-1}k_2^{-n_2-1}\omega^{-n-1}c_jP_j^N/N! \tag{A18}$$

into sums over powers of k_1, k_2, and ω only [thus eliminating P_j using the relations in (A17)]; this gives the alternative expression

$$\mathscr{I}=\frac{\pi^{3/2}}{4}\sum_{M_1}\sum_{M_3}d_j\prod_{i=1}^{3}k_i^{M_i}\Big/\left[\Gamma\left[\frac{M_i+l_i+3}{2}\right]\times\Gamma\left[\frac{M_i-l_i+2}{2}\right]\right]. \tag{A19}$$

In Eq. (A19) ω is relabeled k_3 and

$$M_2=-(M_1+M_2+3)\ ,$$
$$d_1=(-i)^{l_1+l_2+L},\quad d_3=(-i)^{l_1-l_2+L}(-1)^{M_2}\ , \tag{A20}$$
$$d_2=(-i)^{-l_1+l_2-L}(-1)^{M_1+1},\quad d_4=(-i)^{L-l_1-l_2}(-1)^{M_3}\ .$$

The range of sums M_1 and M_3 are finite being limited to terms in which no denominator gamma functions have arguments which would be negative integers.

APPENDIX B: PLANE WAVE CALCULATION OF VIRTUAL PHOTON SPECTRUM

The virtual photon spectrum for multipole order λL broken down into magnetic substates M is defined in a general manner in Eq. (15) in the main text. However, as remarked in the same section, we also need explicit expressions for the same quantities evaluated in the long-wavelength zero-charge limit, $[N_M^{\lambda L}]_0$. Calculation of these quantities is straightforward but rather long and we confine ourselves to giving the final results here. Details are available in Ref. 23. In the following

$$\zeta_0=(E_1E_2+k_1k_2-m^2)/m\omega\ . \tag{B1}$$

Electric dipole

$$N_0^{E1}=\frac{\alpha}{2\pi k_1^4}[k_1k_2(E_1E_2+3m^2)+m^2\omega(3E_1+E_2)\ln\zeta_0] , \tag{B2}$$

$$N_{\pm1}^{E1}=\frac{\alpha}{4\pi k_1^4}\{k_1k_2(-4E_1^2-E_1E_2+m^2)+[2E_1^2(k_1^2+k_2^2)-m^2\omega^2]\ln\zeta_0\} . \tag{B3}$$

Magnetic dipole

$$N_0^{M1}=\frac{\alpha}{2\pi k_1^4}[k_1k_2(E_1E_2-m^2)-m^2\omega^2\ln\zeta_0] , \tag{B4}$$

$$N_{\pm1}^{M1}=\frac{\alpha}{4\pi k_1^4}\{k_1k_2(m^2-E_1E_2)+[2E_1^2(E_1^2+E_2^2)-m^2(E_1+E_2)^2-4m^2k_1^2]\ln\zeta_0\} . \tag{B5}$$

Electric quadrupole

$$\begin{aligned}N_0^{E2}=\frac{\alpha k_2}{4\pi k_1}\{&[12m^6+20m^4E_2^2-28m^4E_1E_2-12m^4E_1^2+12m^2E_1E_2^3\\&+74m^2E_1^2E_2^2-208m^2E_1^3E_2+126m^2E_1^4+6E_1^3E_2^3-4E_1^4E_2^2+2E_1^5E_2]/(3\omega^2k_1^4)\\&+m^2E_1(-8m^2E_2+16m^2E_1-3E_1E_2^2-10E_1^2E_2+5E_1^3)\ln\zeta_0/(k_1^5k_2)\}\end{aligned} , \tag{B6}$$

$$\begin{aligned}N_{\pm1}^{E2}=\frac{\alpha k_2}{8\pi k_1}&[16m^6-22m^4E_2^2+76m^4E_2E_1-70m^4E_1^2-10m^2E_1E_2^3-110m^2E_2^2E_1^2\\&+218m^2E_2E_1^3-114m^2E_1^4-14E_2^3E_1^3+12E_2^2E_1^4+18E_2E_1^5]/(3\omega^2k_1^4)\\&+[2(-4m^6+4m^4E_2^2+10m^4E_2E_1-15m^4E_1^2+m^2E_2^2E_1^2+14m^2E_2E_1^3-11m^2E_1^4+2E_2^2E_1^4+2E_1^6)\ln\zeta_0]/(k_1^5/k_2)\end{aligned} , \tag{B7}$$

$$\begin{aligned}N_{\pm2}^{E2}=\frac{\alpha k_2}{8\pi k_1}\{&[4m^6+2m^4E_2^2-16m^4E_2E_1+18m^4E_1^2-2m^2E_2^3E_1+36m^2E_2^2E_1^2\\&-74m^2E_2E_1^3+20m^2E_1^4+8E_2^3E_1^3-8E_2^2E_1^4+12E_2E_1^5]/(3\omega^2k_1)\\&+[2m^2(m^2E_2^2-2m^2E_2E_1+9m^2E_1^2-2E_2^2E_1^2-4E_2E_1^3-2E_1^4)\ln\zeta_0]/(k_1^5k_2)\}\end{aligned} . \tag{B8}$$

[1]R. O. Haxby, W. E. Shoupp, W. E. Stephens, and W. H. Wells, Phys. Rev. **59**, 57 (1941).

[2]B. Arakatsu, Y. Uemura, M. Sonada, S. Shimizu, K. Kimura, and K. Muraoka, Proc. Phys.—Math. Soc. Jpn. **23**, 440 (1941).

[3]J. T. Caldwell, E. J. Dowdy, B. L. Berman, R. A. Alvarez, and P. Meyer, Phys. Rev. C **21**, 1215 (1980).

[4]A. Veyssiare, H. Beil, R. Bergere, P. Carlos, A. Lapretre, and K. Kernbath, Nucl. Phys. **A199**, 45 (1973).

[5]J. D. T. Arruda-Neto and B. L. Berman, Nucl. Phys. **A349**, 483 (1980).

[6]J. D. T. Arruda-Neto, S. B. Berdale, B. S. Bhandari, and I. C. Nascimento, Phys. Rev. C **14**, 1499 (1976).

[7]J. Aschanbach, R. Haeg, and H. Krieger, Z. Phys. A **292**, 285 (1971).

[8]H. Stroher, R. D. Fisher, J. Drexler, K. Huber, U. Kniessel, R. Ratzek, H. Ries, W. Wilke, and H. J. Maier, Nucl. Phys. **A378**, 237 (1982).

[9]K. Van Bibber, P. Countryman, K. A. Griffioen, D. H. H. Hoffmann, K. T. Knopfle, M. R. Yearian, J. G. Woodworth, D. Rowley, and J. R. Calarco, *Lectures Notes in Physics*, Vol. 158 (Springer, Berlin, 1982), p. 278.

[10]D. H. Dowell, L. S. Cardman, P. Azel, G. Bolme, and S. E. Williamson, Phys. Rev. Lett. **49**, 113 (1982).

[11]W. W. Gargaro and D. S. Onley, Phys. Rev. C **4**, 1032 (1971).
[12]P. Durgapal and D. S. Onley, Phys. Rev. C **27**, 523 (1983).
[13]C. W. Soto Vargas, D. S. Onley, and L. E. Wright, Nucl. Phys. **A288**, 45 (1977).
[14]J. A. Thie and E. Guth, Phys. Rev. **87**, 962 (1952).
[15]R. H. Dalitz and D. R. Yennie, Phys. Rev. **105**, 1598 (1957).
[16]J. R. Woodworth, D. Rowley, J. D. T. Arruda-Neto, P. J. Countryman, K. A. Griffioen, D. H. H. Hoffmann, K. T. Knopfle, K. Van Bibber, M. R. Yearian, and J. R. Calarco, Phys. Lett. **153B**, 226 (1985).
[17]J. M. Blatt and V. F. Weisskopf, *Theoretical Nuclear Physics* (Wiley, New York, 1952).
[18]T. Weber, J. Drexler, R. D. Heil, K. Huber, U. Kneissl, G. Mark, H. Reis, H. Stoker, and W. Wilke, Z. Phys. A **315**, 125 (1984).
[19]J. D. T. Arruda-Neto, S. B. Herdade, I. C. Nascimento, and B. L. Berman, Nucl. Phys. **A389**, 378 (1982).
[20]J. F. Prewitt and L. E. Wright, Phys. Rev. C **9**, 2033 (1974).
[21]H. Uberall, *Electron Scattering from Complex Nuclei* (Academic, New York, 1971).
[22]M. Abramowitz and I. A. Stegun, *Handbook of Mathematical Functions* (Dover, New York, 1972).
[23]F. Zamani-Noor, Ph.D. dissertation, Ohio University, 1984.